Chapter 4

TRANSPORT REGIMES BEYOND DIFFUSION AND THEIR APPLICATIONS

Chapter 4 has been adapted from

(*1*) Chengyun Hua and Austin J. Minnich. "Transport regimes in quasiballistic heat conduction". In: *Phys. Rev. B* 89 (9 2014), p. 094302. DOI: 10.1103/PhysRevB.89.094302. URL: http://link.aps.org/doi/10.1103/PhysRevB.89.094302.

4.1 Introduction

One advantage of analytical solutions to the phonon Boltzmann transport equation (BTE) is that just by looking at the form of the solution we could fully investigate heat conduction from diffusive to ballistic regimes as well as the transition regime, called quasiballistic transport.

Quasiballistic heat conduction occurs if a temperature gradient exists over length scales comparable to phonon mean free paths (MFPs).(*21*, *22*) In this regime, local thermal equilibrium does not exist and Fourier's law is no longer valid. Presently, quasiballistic transport is under investigation due to its potential to infer information about the MFPs of thermal phonons,(*118*) knowledge of which is crucial to engineer thermal conductivity but remains unknown for most solids.(*13*, *14*)

Quasiballistic transport was originally observed in macroscopic samples using heat pulse experiments(*18*) and later in silicon membranes using a microfabricated platform.(*122*) Nonlocal theories of heat conduction based on the BTE were introduced to describe the quasiballistic regime for phonons(*68*, *123*, *124*) and electrons.(*125*) Koh and Cahill reported modulation-frequency dependent thermal conductivities in a time-domain transient thermoreflectance (TDTR) experiment that they attributed

to quasiballistic transport and suggested that the meansurements could be used to measure MFPs. Recently, quasiballistic transport has been observed in other experimental configurations.(*20*, *23–25*) Minnich introduced a reconstruction technique that described how to quantitatively recover the MFP spectra from observations of quasiballistic heat transfer.(*118*)

One notable experimental method for observing quasiballistic transport is the transient thermal grating (TTG) technique(*25*, *126*, *127*), in which the interference of two laser pulses creates a sinusoidal initial temperature profile with wavelength λ. The observed thermal decay yields information about the thermal properties of the material. Recent work has demonstrated that these measurements can also reveal MFPs if the grating wavelength is comparable to MFPs, but interpreting measurements using the reconstruction method introduced by Minnich requires a solution of the BTE. A previous work reported a modified "two-channel" model(*126*), in which low and high frequency phonons are described by the BTE and heat equation, respectively, but the extent of the validity of this model is unclear. An analysis within the framework of the BTE(*128*) has been recently reported but the analysis of the frequency-dependent BTE was solely numerical, complicating its use for the reconstruction method.

Here, we analyze thermal transport in TTG using the Green's function solution to the frequency-dependent BTE derived in Chapter 3. Our analysis demonstrates the existence of weakly and strongly quasiballistic transport regimes that are distinguished by the thermal decay time relative to the phonon relaxation times. We provide theoretical justification for the use of a modified diffusion theory to interpret observations of quasiballistic transport. Finally, we use our solution to derive a corrected suppression function that enables phonon MFP spectra to be measured more accurately. Our results will lead to a better understanding of phonon heat conduction in solids like thermoelectrics.

4.2 Modeling

We start with Eq. 3.1. Thermal transport in a TTG experiment, assuming only in-plane heat conduction and a small temperature rise, $\Delta T = T(x,t) - T_0$, relative to a reference temperature T_0, is described by the 1D frequency-dependent BTE,(*22*)

$$\frac{\partial g_\omega}{\partial t} + v_g \mu \frac{\partial g_\omega}{\partial x} = -\frac{g_\omega}{\tau_\omega} + \frac{1}{4\pi}\frac{C_\omega}{\tau_\omega}\Delta T + \frac{Q_\omega}{4\pi} \tag{4.1}$$

where $g_\omega = f_\omega(x,t,\mu) - f_0(T_0)$ is the deviational distribution function, $f_0 = f_0(x,t)$ is the equilibrium distribution function, $\mu = cos(\theta)$ is the directional cosine, v_ω is the phonon group velocity, τ_ω is the phonon relaxation time, and Q_ω is the spectral volumetric heat generation.

As treated in Chapter 3, to close the problem, energy conservation is used to relate g_ω to ΔT, given by

$$\int \int_0^{\omega_m} \left[\frac{g_\omega(x,t)}{\tau_\omega} - \frac{1}{4\pi}\frac{C_\omega}{\tau_\omega}\Delta T(x,t) \right] d\omega d\Omega = 0, \tag{4.2}$$

where $g_\omega = \hbar\omega D(\omega)(f_\omega(x,t,\theta) - f_0(T_0))$ is the desired deviational distribution function, $Q_\omega(x,t)$ is the spectral volumetric heat generation, $v_g(\omega,T)$ is the phonon group velocity, and $\tau(\omega,T)$ is the phonon relaxation time. Here, x is the spatial variable, t is the time, ω is the phonon frequency, T is the temperature, and $\mu = cos(\theta)$ is the directional cosine of the polar angle θ. $\hbar$ is the reduced Planck constant, $D(\omega)$ is the phonon density of states, f_{BE} is the Bose-Einstein distribution, and $C_\omega = \hbar\omega D(\omega)\frac{\partial f_{BE}}{\partial T}$ is the mode specific heat. The volumetric heat capacity is then given by $C = \int_0^{\omega_m} C_\omega d\omega$ and the thermal conductivity $k = \int_0^{\omega_m} k_\omega d\omega$, where $k_\omega = \frac{1}{3}C_\omega v_\omega \Lambda_\omega$ and $\Lambda_\omega = \tau_\omega v_\omega$ is the phonon MFP.

Since the initial temperature profile in TTG is sinusoidal, we can assume that both g_ω and ΔT are of the form e^{iqx}, where $q = 2\pi/\lambda$ is the grating wavevector, and the volumetric heat generation term in Eq. 4.1 has the following form:

$$Q_\omega = C_\omega e^{iqx}\delta(t), \tag{4.3}$$

where $\delta(t)$ denotes an impulse at $t = 0$, and the initial heat generation follows a thermal distribution. Substituting $g_\omega = \widetilde{g}_\omega(t,\mu)e^{iqx}$ and $\Delta T = \Delta\widetilde{T}(t)e^{iqx}$ into Eq. (4.1) leads to a first-order ODE for $\widetilde{g}_\omega(t)$. Collins *et. al.*(*128*) obtained an analytical solution by applying a Fourier transform to the grey form of this equation. Here, we extend the Fourier transform method to the frequency-dependent BTE.

Applying the Green's function method described in Section 3.2, we are able to decouple the nonlocal effects and directly obtain the following closed-form expression for the unknown distribution function $\widetilde{g}_\omega$ and transient temperature $\Delta\widetilde{T}$:

$$\mathcal{F}[\widetilde{g}_\omega](\eta) = \frac{1}{4\pi}\frac{C_\omega}{\tau_\omega}\frac{\mathcal{F}[\Delta\widetilde{T}](\eta)}{\gamma - i\eta} + \frac{C_\omega}{4\pi\tau_\omega}\frac{\Delta\widetilde{T}(0)}{\gamma - i\eta} \tag{4.4}$$

$$\mathcal{F}[\Delta\widetilde{T}](\eta) = \frac{\Delta\widetilde{T}(0)\int_0^{\omega_m}\frac{C_\omega}{\tau_\omega}\mathcal{A}(\eta)d\omega}{\int_0^{\omega_m}\frac{C_\omega}{\tau_\omega}[1-\mathcal{A}(\eta)]d\omega} \tag{4.5}$$

$$\mathcal{A}(\eta) = \frac{i}{2q\Lambda_\omega}\log\left(\frac{\tau_\omega\eta + q\Lambda_\omega + i}{\tau_\omega\eta - q\Lambda_\omega + i}\right), \tag{4.6}$$

where $\mathcal{F}$ denotes Fourier transform, $\gamma = (1 + iq\mu\Lambda_\omega)/\tau_\omega$, and η is the temporal Fourier variable. The time-domain solution is obtained by inverse fast Fourier transform. Therefore, we have derived an analytical solution to the frequency-dependent BTE that is valid from the ballistic to the diffusive regimes, enabling a more rigorous understanding of thermal transport in TTG.

We can gain insight into which parameters determine the transport regime from our solution. From Eq. (4.6), we identify two nondimensional parameters. One is the familiar phonon Knudsen number $\mathrm{Kn}_\omega = q\Lambda_\omega$, which compares the phonon MFP with a characteristic length, in this case $1/q$. To identify the second parameter, we notice that η^{-1} describes a time scale that we assign to be the characteristic thermal decay time Γ. We can therefore define a new non-dimensional parameter that we denote the transient number, given by $H_\omega = \tau_\omega/\Gamma$, which compares the phonon relaxation times with the thermal decay time Γ.

Note that the two parameters are not completely independent. For example, as the grating wavelength decreases, the thermal decay time also decreases. In the diffusion regime the relationship is trivial but in the quasiballistic and ballistic regimes the relationship becomes much more complex. While the Knudsen number can in principle completely distinguish the transport regime, we find that the transient number is an additional convenient parameter by which to specify the regime, particularly for quasiballistic transport where the specific Knudsen number at which a transition occurs is not obvious.

Therefore, together, these two numbers completely specify the transport regime. In the diffusive limit, length and time scales are much larger than the phonon MFPs and relaxation times, respectively, corresponding to $\mathrm{Kn}_\omega \ll 1$ and $H_\omega \ll 1$. In the ballistic regime, lengths and times are much smaller than MFPs and relaxation times, or $\mathrm{Kn}_\omega \gg 1$ and $H_\omega \gg 1$. The two regimes are well-understood limits of the BTE(*21*). Here, we focus on the intermediate range of the two limits, the quasiballistic regime.

4.3 Heat transport regimes

To begin, we examine the transient temperature decay in the different regimes as shown in Fig. 4.1. We perform our calculations for crystalline silicon, using the experimental dispersion in the [100] direction and assuming the crystals are isotropic. The numerical details concerning the dispersion and relaxation times are given by Minnich's recent work(*79*).

Diffusive and ballistic limits

We first confirm that our result correctly reproduces the diffusive and ballistic limits. Examining the limit of Eq. (4.5) when both phonon relaxation times and MFPs are much smaller than their corresponding characteristic scales ($H_\omega \ll 1$ & $\mathrm{Kn}_\omega^2 \ll 1$), we find that the solution reduces to the Fourier solution and the thermal decay

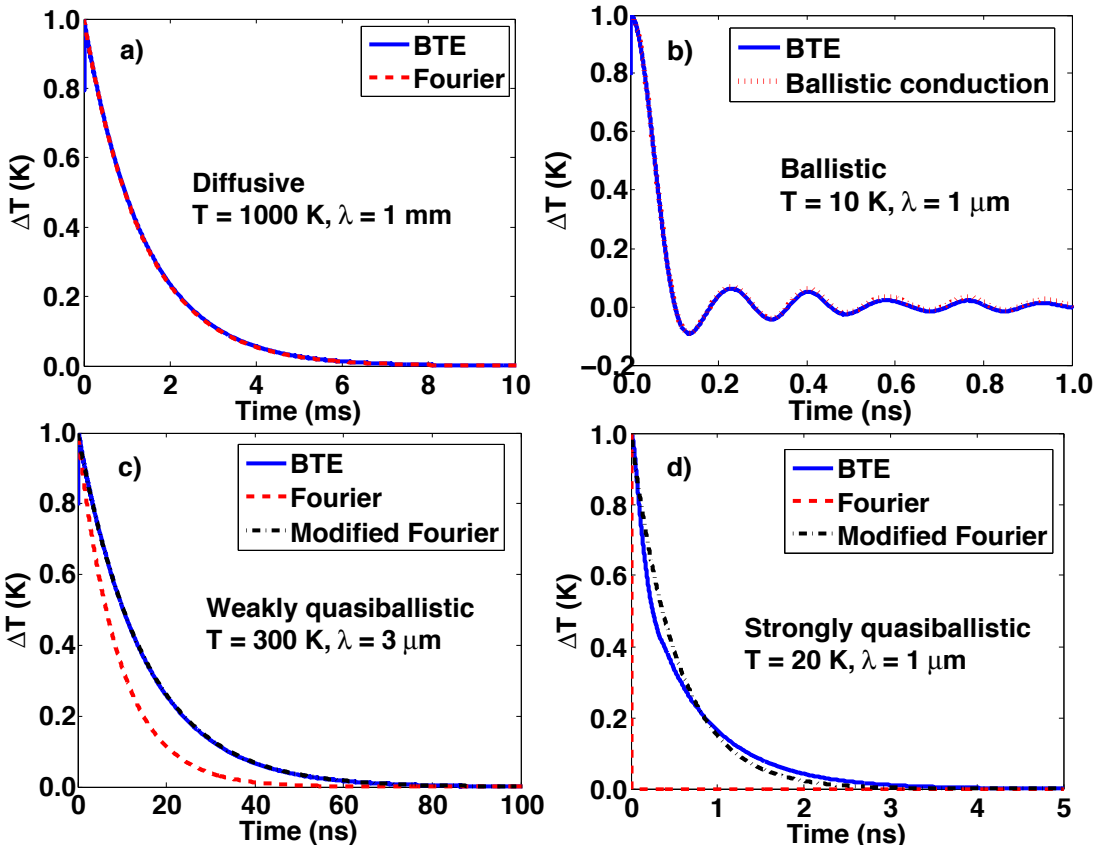

Figure 4.1: Temperature decay curves $\Delta\widetilde{T}$ in the (a) diffusive limit, (b) ballistic limit, (c) weakly quasiballistic regime, and (d) strongly quasiballistic regime. The BTE solutions are given by the solid lines, the Fourier solution by the dashed lines, the ballistic conduction solution by the dotted line, and the Modified Fourier solution by the dash-dotted lines.

time $\Gamma = (q^2\alpha)^{-1}$, where $\alpha = k/C$ is the Fourier thermal diffusivity. Fig. 4.1(a) demonstrates that the BTE solution agrees with the Fourier solution in this limit. Similarly, at the ballistic limit ($H_\omega \gg 1$ & $\mathrm{Kn}_\omega^2 \gg 1$) shown in Fig. 4.1b, the transient temperature given by Eq. (4.5) agrees with the ballistic solution of the BTE in which the relaxation times go to infinity.

Weakly quasiballistic regime

We now examine the intermediate quasiballistic regime by allowing the MFPs to be comparable to or greater than the grating wavevector while requiring the thermal decay time to be much longer than relaxation times, $\mathrm{Kn}_\omega^2 \sim 1$ but $H_\omega \ll 1$. We observe that the BTE solution does not agree with the Fourier's law solution, as shown in Fig. 4.1(c). However, we observe that the shape of the temperature decay remains exponential, as in Fourier's law, but with a smaller thermal conductivity. We denote this regime the weakly quasiballistic regime, and the Fourier solution with a modified thermal conductivity as the modified Fourier solution. So far, the validity of the modified Fourier model to describe quasiballistic thermal transport is largely based on experimental observations.(*25*) The only theoretical approach to explain this observation was developed by Maznev *et. al.*(*126*) Their modified "two-channel" model assumes that the low-frequency phonons, which are analyzed by the BTE, only interact with the thermal reservoir of high-frequency phonons, which are analyzed by the diffusion equation. However, the extent of the validity of this assumption is not clear.

Here, we give a more rigorous explanation using our solution. Under the assumption of $\mathrm{Kn}_\omega^2 \sim 1$ and $H_\omega \ll 1$, the Taylor expansion of Eq. 4.6 around $H_\omega = 0$ gives

$$\mathcal{A}(\eta) = i\eta_\omega\eta + \frac{\tan^{-1}(\mathrm{Kn}_\omega)}{\mathrm{Kn}_\omega} \sim 1. \tag{4.7}$$

We observe that in the denominator of Eq. (4.5), $1 - \mathcal{A}(\eta) \sim \tau_\omega$ and the full asymp-

totic expression of $\mathcal{A}(\eta)$ should be used while in the numerator, $\mathcal{A}(\eta)$ can be approximated 1. Therefore, Eq. (4.5) asymptotically approaches the following form:

$$\mathcal{F}[\Delta\widetilde{T}](\eta) \approx \frac{\Delta\widetilde{T}(0)}{q^2\alpha_{mod} - i\eta} \tag{4.8}$$

$$k_{mod} = \int_0^{\omega_m} k_\omega \left\{ \frac{3}{(\mathrm{Kn}_\omega)^2} \left[1 - \frac{\tan^{-1}(\mathrm{Kn}_\omega)}{\mathrm{Kn}_\omega} \right] \right\} d\omega, \tag{4.9}$$

where $\alpha_{mod} = k_{mod}/C$ is the apparent thermal diffusivity and k_{mod} is the modified thermal conductivity. Recognizing that Eq. (4.8) is simply the Fourier transform of an exponential decay, we find $\Delta\widetilde{T}(t) \approx \Delta\widetilde{T}(0)\exp\left(-q^2\alpha_{mod}t\right)$. Thus, the formal solution of the BTE is equivalent to a modified diffusion theory with a modified thermal conductivity given by Eq. (4.8). The thermal decay time $\Gamma = (q^2\alpha_{mod})^{-1}$. We term this simplified solution the weak solution to the BTE, valid in the weakly quasiballistic regime. The modified thermal conductivity is the same expression given by Maznev *et. al.*(*126*)

Most recent experimental observations of quasiballistic transport have occurred in this weakly quasiballistic regime. For instance, in the TTG measurement of silicon membranes reported by Johnson *et al.*,(*25*) the typical $\mathrm{Kn}_\omega \approx 2.5$ and $H_\omega \sim O(0.01)$, based on the median thermal phonon MFP at the room temperature. Therefore, their measurements fall into the weakly quasiballistic regime and a modified Fourier solution should explain the results, in agreement with the experiment.

Strongly quasiballistic regime

As the grating wavelength decreases, eventually the thermal decay becomes so fast that it is comparable to or greater than relaxation times such that $H_\omega \sim 1$ and $\mathrm{Kn}_\omega^2 \sim 1$. Here, the assumption made in the modified "two-channel" model is not valid because some phonons in the thermal reservoir are now ballistic. For silicon, this regime occurs at small grating wavelength ($\lesssim 0.5\ \mu m$) or at cryogenic temper-

atures. In this case, the BTE solution deviates from the exponential decay and can no longer be explained with any type of diffusion model as shown in Fig. 4.1d, and a full solution given by Eq. (4.5) is necessary. We denote this regime the strongly quasiballistic regime. The equivalent decay time Γ is given by $\int_0^\infty \Delta T(t)dt/\Delta T(0)$, which reduces to the corresponding thermal decay times in the other two regimes above.

4.4 Suppression function

We now seek to understand how the thermal length and time scales affect which phonons conduct heat in each regime. From our model, we can calculate the spectral thermal conductance, defined as the ratio of heat flux to the temperature difference

$$\sigma_\omega = \frac{\int\int q_\omega(x,t)dxdt}{\int\int \Delta T(x,t)dxdt} = \frac{\int\int \widetilde{q}(\eta)e^{iqx}dxd\eta}{\int\int \Delta\widetilde{T}(\eta)e^{iqx}dxd\eta}, \tag{4.10}$$

where $q_\omega(x,t) = \int g_\omega(x,t,\theta)v_\omega \cos(\theta)d\Omega$ is the spectral heat flux. In this way, we remove any spatial and temporal factors and can directly compare the heat flow induced by a unit temperature difference for each phonon mode.

Substituting Eqs. (4.4) & (4.5) into Eq. (4.10), we derive a general expression for the spectral thermal conductance

$$\sigma_\omega = \sigma_f \left\{ \frac{3}{(\mathrm{Kn}_\omega)^2} \left[1 - \frac{\tan^{-1}(\mathrm{Kn}_\omega)}{\mathrm{Kn}_\omega} \right] [H_\omega + 1] \right\}, \tag{4.11}$$

where $\sigma_f = k_\omega/(\lambda/2)$ is the Fourier thermal conductance. The term in the brackets, equal to the ratio of the BTE thermal conductance to the Fourier thermal conductance, was previously termed the suppression function $S(\mathrm{Kn}_\omega, H_\omega)$ by Minnich(*118*).

Now let us examine the thermal conductance in the two quasiballistic transport regimes discussed above, shown in Fig. 4.2. We compare the thermal conductance calculated by the Fourier's law, weak BTE and full BTE solutions.

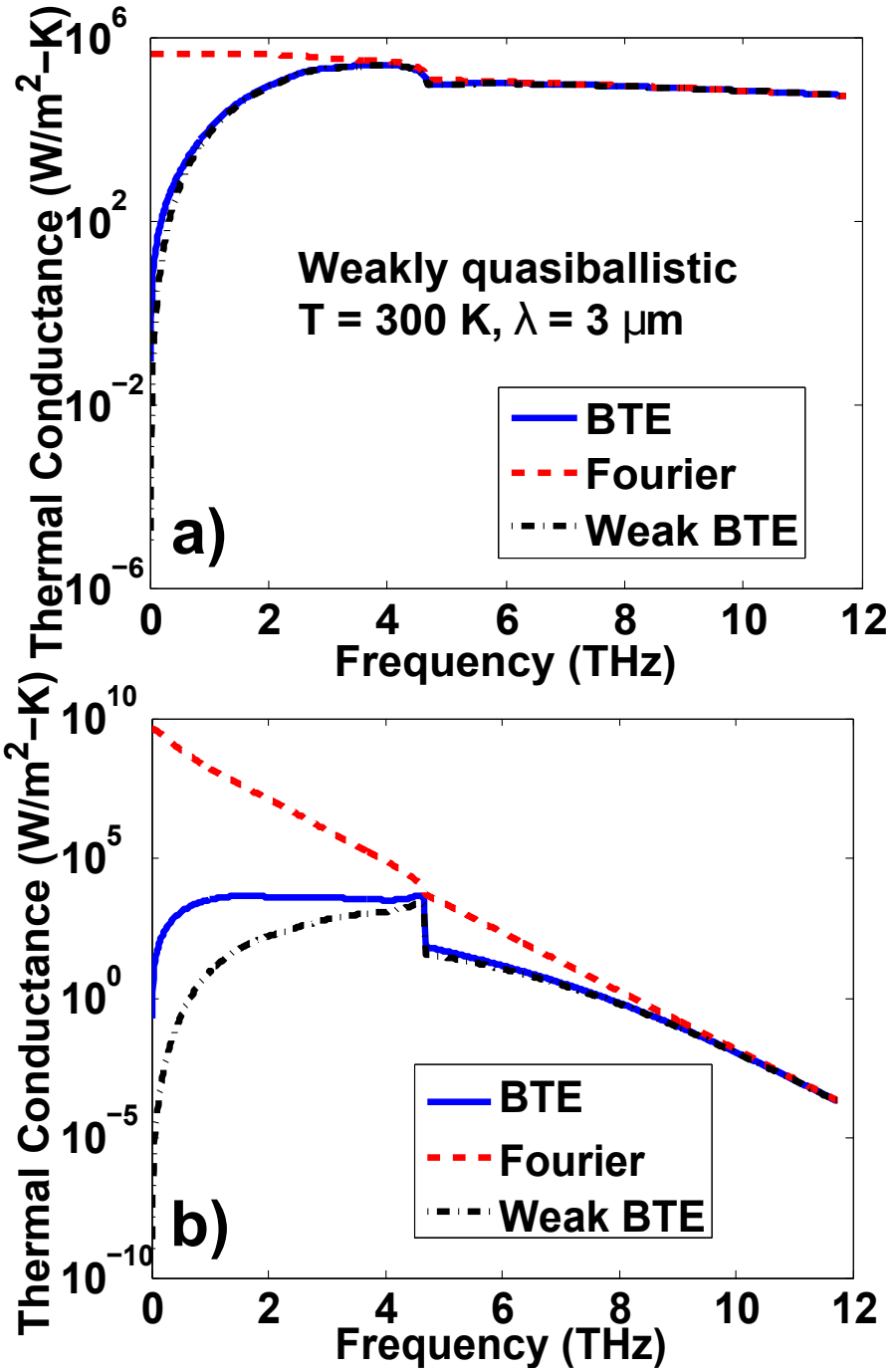

Figure 4.2: Spectral thermal conductance σ_ω in the (a) weakly quasiballistic regime and (b) strongly quasiballistic regime. The BTE solutions are given by the solid lines, the Fourier solution by the dashed lines, and the weak BTE solution by the dash-dotted lines.

In weakly quasiballistic regime, where $\mathrm{Kn}_\omega^2 \sim 1$ but $H_\omega \ll 1$ (Fig. 4.2(a)), $H_\omega + 1 \rightarrow 1$ and Eq. (4.11) reduces to $\sigma_\omega = \sigma_f S_{weak}(\mathrm{Kn}_\omega)$, where $S_{weak}(\mathrm{Kn}_\omega)$ is the same as the term in the brackets of Eq. (4.9). In this regime, Fourier's law overpredicts the heat flux but the weak BTE solution still accurately describes the spectral heat distribution. From Fig. 4.2(b), we see that the heat contribution from low frequency phonons is suppressed compared to the Fourier's law prediction.

In the strongly quasiballistic regime (Fig. 4.2(b)), the weak BTE solution does not accurately explain the spectral conductance and we must instead use Eq. (4.11). The full BTE solution predicts a more gradual suppression than the weak BTE solution for those low frequency phonons whose relaxation times are comparable to or greater than the thermal decay time Γ. This discrepancy is due to the correction term $H_\omega + 1$, which approaches its maximum value at low frequencies and reduces the suppression effects. Rewriting H_ω into $\Lambda_\omega/(v_\omega\Gamma)$ in Eq. (4.11), we find that our new suppression function decreases as $1/\Lambda_\omega$ in the long MFP limit, in agreement with the ballistic limit of the BTE(*21*) while $S_{weak}(\mathrm{Kn}_\omega)$ predicts a steeper slope, $1/\Lambda_\omega^2$, which is inconsistent with the ballistic limit. Therefore, our new suppression function provides a more accurate prediction of the heat flux suppression over the entire spectrum of phonons compared to the approximate approaches in the literature.(*126*, *128*)

4.5 Application

We now show the utility of these insights by demonstrating how our new suppression function may be used to more accurately measure MFP spectra. As proposed by Minnich(*118*), the apparent thermal conductivities can be related to the MFP distribution by the equation $k_{app} = \int_0^\infty S(\Lambda_\omega) f(\Lambda_\omega) d\Lambda_\omega$ where $S(\Lambda_\omega)$ is the suppression function, the phonon MFP Λ_ω is the independent variable and $f(\Lambda_\omega)$ is the desired MFP distribution. If the apparent thermal conductivities are experimentally

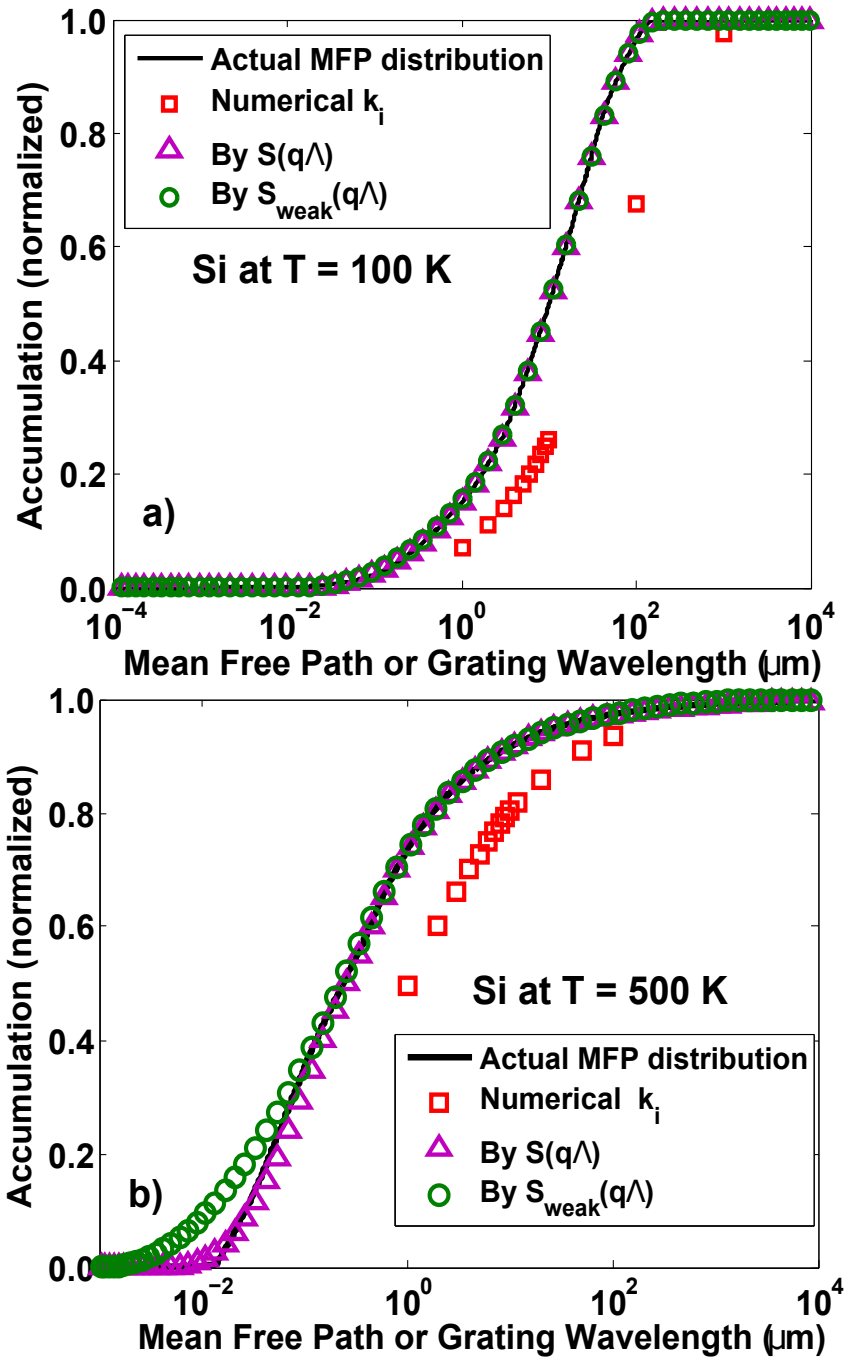

Figure 4.3: Example MFP reconstructions for silicon at (a) 100 K and (b) 500 K using numerically simulated data. Plotted are the analytical MFP distribution (solid line), the numerical apparent thermal conductivities (squares), the reconstructed MFP distributions by the general suppression function (triangles) and by the weak suppression function (circles). The x-axis corresponds to the MFP for the distributions and to the grating wavelength for the thermal conductivity data.

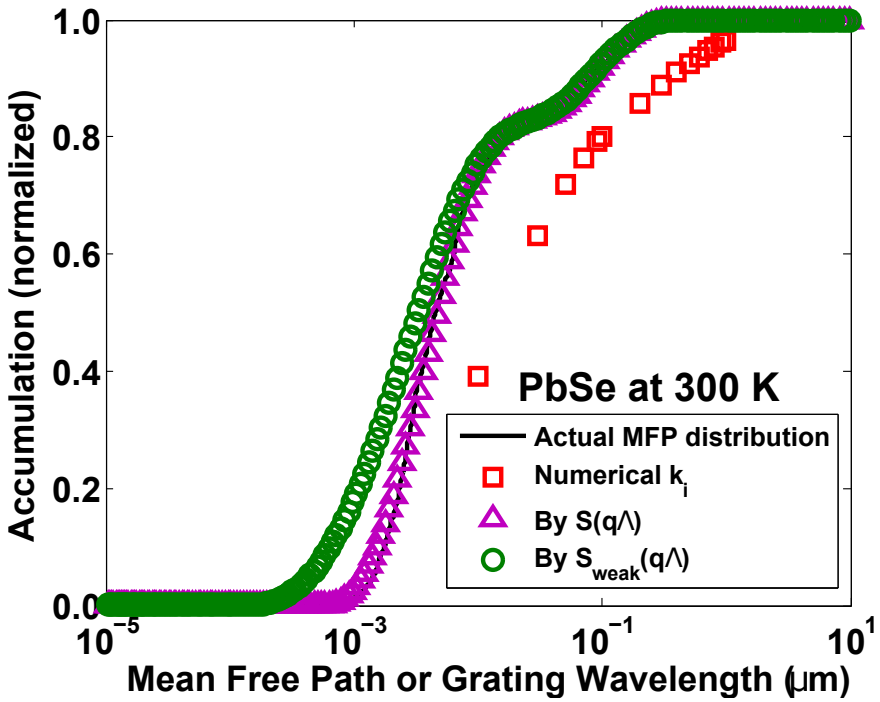

Figure 4.4: Example MFP reconstructions for PbSe at 300 K using numerically simulated data. Plotted are the analytical MFP distribution (solid line), the numerical apparent thermal conductivities (squares), the reconstructed MFP distributions by the general suppression function (triangles) and by the weak suppression function (circles). The x-axis corresponds to the MFP for the distributions and to the grating wavelength for the thermal conductivity data.

measured and the suppression function is known, then the MFP distribution can be reconstructed by solving the integral equation as an inverse problem.

From our analysis, we have already derived the necessary suppression function $S(\mathrm{Kn}_\omega, H_\omega)$ in Eq. (4.11). However, this suppression function depends both on the independent variable, the phonon MFP Λ_ω, as well as the unknown relaxation time τ_ω. To perform the reconstruction, Λ_ω should be the only unknown variable.

To overcome this problem, we rewrite τ_ω into Λ_ω/v_ω and assume that the phonon group velocity v_ω is equal to the average sound velocity v_s. This assumption is

justified since for long MFP phonons for which the correction term is important, the group velocity of phonons is close to the sound speed, while for short MFP phonons this term is negligible and the choice of the velocity is irrelevant. The reconstruction is also insensitive to the precise choice of the value of v_s. For example, for PbSe, changing v_s from 2000 m/s to 1000 m/s causes only a 10 % maximum error in the reconstructed MFP distribution. Using this approximation, the suppression function is only a function of the independent variable Λ_ω.

To demonstrate the inversion procedure using this new suppression function, we perform numerical experiments in which we obtain the modified thermal conductivities of Silicon and PbSe at different temperatures for different grating wavelengths from the temperature decay curves predicted by the BTE. These modified thermal conductivities, along with the suppression function, are then used as inputs for the reconstruction procedure. Figs. 4.3 & 4.4 show the results of the MFP reconstruction for Si and PbSe using the general and weak suppression functions.

For materials with a MFP spectrum that is in the range of the experimental length scales, such as Silicon at 100 K, the measurements of the apparent thermal conductivities at different grating wavelengths span almost the entire range of phonon MFP spectrum. In this case, as shown in Fig. 4.3(a), both the weak and new suppression functions yield satisfactory results. However, phonon MFPs vary by orders of magnitude and some part of the spectrum may be inaccessible to experiment. For example, the smallest MFPs of Silicon at 500 K are around 10 nm and the smallest MFPs of PbSe at room temperature are around 1 nm. These length scales are too small to be accessed with present experimental methods, meaning the MFP distribution at small length scales must be extrapolated from measurements at larger length scales. Such an extrapolation requires evaluating the suppression function at large values of the argument, precisely in the range where the correction term to the new suppression function is important. As shown in Figs. 4.3(b) and 4.4,

our new suppression function yields more accurate results at short MFPs while the weak suppression function overpredicts the MFP distribution.

4.6 Summary

We have analyzed thermal transport in TTG using the Green's function solution to the frequency-dependent BTE. We identify the thermal decay time relative to the relaxation times as a key nondimensional parameter that separate two quasiballistic transport regimes. If the thermal decay time is much larger than relaxation times, a modified diffusion theory is the formal solution of the BTE, providing theoretical justification for prior interpretations of experimental observations of quasiballistic transport. Further, we demonstrate how MFP spectra may be measured more accurately using our new suppression function.

Now we have both the theoretical tools and experimental techniques to study the microscopic transport processes of thermal phonons in bulk materials. In the next chapter, we will demonstrate a general route to directly study the microscopic transport processes at solid-solid interfaces using experiments. With both approaches, we will be able to obtain a comprehensive picture of nanoscale energy transport in solids.